Sources and Long-term Variability of Carbon Monoxide at Mount Kenya and in Nairobi

Leonard Kirago[1], Örjan Gustafsson[1], Samuel M. Gaita[1], Sophie L. Haslett[1], Michael J. Gatari[2], Maria E. Popa[3], Thomas Röckmann[3], Christoph Zellweger[4], Martin Steinbacher[4], Jörg Klausen[5], Christian Félix[5], David Njiru[6], and August Andersson[1]*

[1]Department of Environmental Science, and the Bolin Centre for Climate Research, Stockholm University, 10691 Stockholm, Sweden
[2]Institute of Nuclear Science & Technology, University of Nairobi, 31907-00100 Nairobi, Kenya
[3]Institute for Marine and Atmospheric research Utrecht (IMAU), Utrecht University, Utrecht 3584CC, The Netherlands
[4]Empa, Swiss Federal Laboratories for Materials Science and Technology, Laboratory for Air Pollution/Environmental Technology, 8600 Dubendorf, Switzerland
[5]Federal Office of Meteorology and Climatology MeteoSwiss, CH-8058 Zurich, Switzerland
[6]Kenya Meteorological Department, Nairobi, Kenya

*_Correspondence to_: August Andersson (august.r.andersson@gmail.com)

Abstract. Carbon monoxide (CO) concentrations in the troposphere are decreasing globally, with Africa as an exception. Yet, the region is understudied, with a deficit of ground-based observations and highly uncertain CO emission inventories. This paper reports multi-year observational CO data from the Mt. Kenya Global Atmosphere Watch (GAW) station, as well as summertime CO isotope observations from both Mt. Kenya and Nairobi, Kenya. The CO variability at Mt. Kenya is characterized by slightly increased concentrations during dry periods and a strong influence of short-term pollution events. While some data gaps and differences in instrumentation complicate decadal-scale trend analy-sis, a small long-term increase is resolved. ~~While multi-year data gaps complicate decadal-scale trend analysis, no overall long-term shift can be resolved.~~ High pollution events are consistent with isotopic signal from downwind savanna fires. The isotope fingerprint of CO in Nairobi indicate an overwhelming dominance (near 100%) of primary emissions from fossil fuel combustion - with implications for air pollution policy. In contrast, the isotope signature of CO intercepted at the large footprint Mt. Kenya region suggests at least 70% primary sourced, with a predominance likely from, savanna fires in Africa. Taken together, this study provides quantitative constraints of primary vs secondary CO in the eastern Africa region and in urban Nairobi, with implications for satellite-based emission inventories as well as for chemical-transport and climate-modelling.

1. Introduction

Carbon monoxide (CO) is the dominant sink for the hydroxyl radical (OH), accounting for over 50% consumption of OH in the atmosphere (Lelieveld et al., 2016). It therefore influences the atmosphere's oxidation and cleansing capacity and, by extension, chemically regulates the atmospheric lifetime and abundance of other reactive gases such as methane and halocarbons (Lelieveld et al., 2016; Zheng et al., 2019). As such, CO is an indirect greenhouse gas with a net positive warming effect on climate (Szopa et al., 2021). In addition to climate effects, CO is a precursor to the formation of ground-level ozone, with implications for human health (Chen et al., 2021; WHO, 2016; Zhang et al., 2019). Anthropogenic activities such as biomass burning and fossil fuel combustion are important contributors to the global CO budget, in addition to atmospheric reactions, e.g., oxidation of hydrocarbons (Duncan et al., 2007; Zheng et al., 2019). However, the CO source contributions, mole fractions, and atmospheric residence time are spatially variable, complicating the source-sink assessment.

Global CO levels have been declining over the past two decades, but Africa is an exception. The key source of information on CO trends in the African region is satellite-based observations that show an increase in CO mole fractions (Buchholz et al., 2021; Hedelius et al., 2021; Zheng et al., 2019). However, the ground-truthing of the satellite observations is challenged by a deficit of atmospheric observatories and scant continuous long-term observations in the region (DeWitt et al., 2019; Henne et al., 2008b; Kulmala, 2018). Exacerbating this observational deficit, regional CO emission inventories are not well-defined as the continent possesses a unique CO emission profile, different from other regions such as Europe and South Asia (Crippa et al., 2018; Dasari et al., 2022; Hedelius et al., 2021). To advance our understanding of trends in CO over Africa and its source contributions, long-term CO measurements and isotope-based source apportionment studies are required but data availability is scarce.

The isotopic composition of CO provides insights into the relative strengths of regional CO sources and atmospheric processing (Brenninkmeijer, 1993; Dasari et al., 2022; Henne et al., 2008b; Röckmann et al., 2002). A particular source of CO possesses a characteristic isotopic signature, with the isotopic composition of the ambient CO reflecting that of the combined sources, sinks, and atmospheric ageing (Brenninkmeijer and Röckmann, 1997; Dasari et al., 2022; Popa et al., 2014; Röckmann et al., 1998, 2002). For example, CO from primary sources (fossil combustion and biomass burning) has a more enriched $\delta^{18}O$ signature (above +12‰) compared to that of secondary-formed CO, e.g., from oxidation of CH_4 (at ~0‰) and non-methane hydrocarbons (NMHC), at ~2.4 ± 2.4‰ (Brenninkmeijer and Röckmann, 1997).

Additional source information can be obtained from the $\delta^{13}C$ signatures. CO formed from methane oxidation is strongly depleted in ^{13}C ($\delta^{13}C$ = -51.9 ± 1.6‰) in contrast to, for example, CO emitted from burning of C_4 plants ($\delta^{13}C$ = -14.0 ± 3.8‰), C_3 plants ($\delta^{13}C$ = -26.9 ± 4.9‰) or fossil combustion at -27.8 ± 1.5‰ (Brenninkmeijer et al., 1999). However, the kinetic isotope effect (KIE) during the CO-OH reaction (the main atmospheric CO removal mechanism) results in the enrichment of $\delta^{13}C$ by 4-5‰ and more depleted $\delta^{18}O$ signatures (by ~10‰) in the lower troposphere (Brenninkmeijer et al., 1999; Röckmann et al., 1998). Overall, isotope forensics can provide valuable data on CO emissions in remote and urban locations in Africa, especially considering that the region is largely understudied, with very few ground-based CO observations and highly uncertain emission inventories.

This study investigates the long-term trends in CO mole fractions at Mt. Kenya GAW station, a high-altitude monitoring site in equatorial East Africa well suited to intercept the regional emission footprint. Online CO mole fractions measurements have been going on at the observatory since 2002, albeit with large data gaps due to technical challenges. Flask-based measurements carried out at Mt. Kenya at different periods by NOAA (2003-2011) were used for gap filling. The online and NOAA flask-measured CO data were obtained from the WMO's World Data Centre for Greenhouse Gases (WDCGG) database. After the CO measurements from Cape Point, South Africa, this is likely the longest-running data available in sub-Saharan Africa and provides observational constraints of the region's long-term trend in CO. The present study additionally provides stable isotope composition data of CO to resolve source attribution of the observed higher summertime CO amount fraction. Furthermore, the data are compared to previously obtained and unpublished isotope data fromMt. Kenya (1996-1997; earlier unpublished work by Röckmann and Brenninkmeijer) and that of an urban site in Nairobi in summer 2021 to provide further insights into regional CO sources. This dataset is unprecedented in the region and facilitates imporved understanding of the regional CO emission trends and source attribution.

2. Methodology

2.1 Measurement sites

Ambient air sampling was conducted at a remote mountain site, the Mt. Kenya Global Atmospheric Watch (GAW) station, and in Nairobi city. The Mt. Kenya GAW station is located on the north-western slope of Mt. Kenya (0.062 °S, 37.297 °E, at 3678 m MSL) in eastern equatorial Africa. The station description, site selection and representativeness, and meteorological characterization are detailed by Henne et al. (2008a, 2008b). In brief, the station lies within a nature conservancy, the Mount Kenya National Park, and contributes to the World Meteorological Organization GAW programme. The closest human settlements and roadways are over 17 km away, and the nearest town (Nanyuki) is at 1900 m MSL. A small touristic infrastructure, the Old Moses Camp, is situated 300 m below and ca. 1.9 km to the NNW of the station. The second site, in the megacity of Nairobi, Kenya, was a rooftop measurement site (~17 m above ground level; 1690 m asl.; 1.279° S, 36.817° E). As described previously, the Nairobi site is representative of the city's ambient conditions (Kirago et al., 2022b).

2.2 Ambient air sampling

Glass flask sampling was conducted in August 2021 at the Mt. Kenya GAW station and in Nairobi with an in-house assembled portable sampler consisting of a diaphragm pump (KNF Neuberger N86E) connected with 1/4" Dekabon tubing. The sampler design, glass flask pre-conditioning protocol and sampling procedure are previously described (Dasari et al., 2022). Briefly, the sampler was designed to fill two pre-conditioned glass flasks (Normag, 1L) simultaneously, that is, each sample was collected in duplicates. Ambient air was drawn at a flow rate of 2 L min^{-1} and dried through a magnesium perchlorate trap. First, the glass flasks were flushed for 20 minutes before compressing the dried air to an absolute pressure of ~1.7 bar. At Mt. Kenya GAW station, 21 nighttime (02:00h local time) and six daytime (14:00h local time) air sample sets were collected. Nine sample pairs were collected in Nairobi (every second day; daytime only; 14:00h local time). The filled glass flasks were sent to the Institute for Marine and Atmospheric Research Utrecht (IMAU), Utrecht University, for processing and stable isotope analysis of CO.

2.3 Measurements of CO mole fractions and stable isotopes ($\delta^{18}O$ and $\delta^{13}C$) composition of CO

The CO mole fraction and stable isotopic composition measurements of the collected glass flask samples were performed at IMAU, Utrecht University. A continuous-flow isotope ratio mass spectrometry (CF-IRMS, Thermo Scientific Delta V Advantage) system was used, applying a previously described measurement protocol (Pathirana et al., 2015). In brief, the sample gas was introduced into the analytical system using an automated multi-port unit, via a mass flow controller and under ultra-high-purity helium flow. Here, the air sample was directed through a trap with Ascarite (8 - 20 mesh, Thermo Scientific™) followed by magnesium perchlorate (Sigma-Aldrich), to remove CO_2 and water. A subsequent cryogenic trap (liquid N_2, -196 °C) was used to remove the remaining traces of CO_2, N2O and hydrocarbons. The CO in the clean air matrix was then oxidized to CO_2 using Schütze reagent (I_2O_5/H_2SO_4 mixture on granular silica gel) synthesized in-house. Subsequently, the CO-derived CO_2 was cryo-trapped in liquid-N_2, while other residual gases (e.g., O_2 and N_2) were pumped out. The sample was further purified on a GC column, dried via a Nafion dryer, and subsequently transferred to the CF-IRMS via an open split inlet for stable isotopes ($\delta^{18}O$ and $\delta^{13}C$) analysis.(Pathirana et al., 2015) The original CO amount fraction was deduced from the quantity of the derived CO_2.

The isotopic composition is expressed as per mil (‰) enrichment or depletion of the isotope ra-tio in the sample relative to that of international standard materials, which in these cases are the Vienna PeeDeeBelemnite (V-PDB) standard for δ13C-CO, and the Vienna Standard Mean Ocean Water (V-SMOW) for δ18O-CO measurements ~~The isotopic composition is expressed as per mil (‰) enrichment or depletion of the isotope ratio in the sample relative to that of international standard materials, which in these cases are the Vienna PeeDeeBelemnite (V-PDB) standard for $\delta^{13}C$ CO, and the Vienna Standard Mean Ocean Water (V-SMOW) for $\delta^{18}O$ CO measurements~~ (Brenninkmeijer et al., 1999; Pathirana et al., 2015). A reference cylinder with atmospheric air with known isotopic composition and mole fraction ($\delta^{13}C$ = -30.25‰; $\delta^{18}O$ = +7.10‰; CO = 180 ppb) was used for calibration. Periodical measurements of "target" gases were used to monitor the precision and accuracy of the measurements, as well as the long-term stability of the analytical system (Pathirana et al., 2015). In addition, blank runs (without injecting the sample or reference gas) were performed to assess the background CO_2, mainly from the Schütze reagent. The typical 1-sigma measurement reproducibility during the time of these analyses is estimated at 0.12‰ for $\delta^{13}C$ and 0.16‰ for $\delta^{18}O$.

2.4 Sampling and isotopic characterization of CO for the 1996/97 campaign

High-volume air samples were collected between July and September 1996 ~~The 1996/97 high-volume air samples were collected~~ on an exploratory mission around Mount Kenya following the ring road A2/B6, and branching off towards the mountain to locations where sufficient power was available for sample collection. During this campaign and later incidental samplings in 1997 ~~During this campaign and later incidental samplings,~~ air samples of approximately 500 L volume were compressed into 5 L aluminium cylinders using a modified RIX compressor (Mak and Brenninkmeijer, 1994). Unfortunately, records of precise locations have been lost. The filled cylinders were sent to the Max Planck Institute for Chemistry in Mainz, Germany, for CO isotope analysis on a high-volume extraction unit (Brenninkmeijer et al., 1999; Röckmann et al., 2002). A high CO concentration calibration gas (269

ppm) that was used during the 1996/7 measurements has been preserved and is regularly measured in the lab of Utrecht University to assure scale compatibility.

2.5 Long-term CO mole fractions at the Mt. Kenya GAW station

High-resolution CO data from Mt. Kenya GAW station are available from the WMO World Data Centre for Greenhouse Gases (WDCGG; https://gaw.kishou.go.jp/). A continuous time series is available for the 2002-2006 and 2020-2021 periods, with some large gaps attributable mainly to power outages and data quality issues. Between 2010 and 2015, the station was disconnected from the power grid following a bush fire, while performance audits revealed the CO analyzer to be in poor working condition between 2015-2019 (decommissioned in 2020), compromising the data quality (Zellweger et al., 2020). Over time, the CO measurements were made using different CO analyzers (Thermo Electron Corporation TEI 48C-TL in 2002-2006, Horiba APMA360 in 2010-2019, and Picarro G2401 in 2020-2021).

The instrument calibration, quality control protocols, and data treatment procedures are discussed elsewhere (Henne et al., 2008b; Zellweger et al., 2009, 2020). In brief, ambient air was drawn into the CO instrument using 1/4" Teflon (till 2019) and ¼" Synflex 1300 (after 2019) tubings at a flow rate of 4 l/min via a Nafion drier to remove moisture and a partice filter. The air inlet was about 7 m above ground and protected against rain, snow and direct wind. These instruments were installed and calibrated by the Swiss Federal Institute for Materials Science and Technology (Empa) in collaboration with the Federal Office of Meteorology and Climatology MeteoSwiss, and operated by the Kenya Meteorological Department (KMD). The instrument calibration and performance audits are conducted regularly by the GAW World Calibration Center hosted at Empa (Zellweger et al., 2020). In addition, flask-based CO data from Mt. Kenya GAW station by NOAA Global Monitoring laboratory and published in the WDCGG database was used in this study (Petron, 2023).

2.6 Trajectory and statistical modelling

The air mass back trajectories (10 days; arrival height of 100 m above ground level) were calculated to identify the air mass source region. The NOAA Hybrid Single-Particle Lagrangian Integrated Trajectory model (HYSPLIT, version 4) and GDAS (1° × 1°) archived meteorological datasets were used (Stein et al., 2015). The Bayesian Markov chain Monte Carlo (MCMC) model was used to quantitatively constrain CO fractional contributions and account for source end member variability and measurement uncertainties (Dasari et al., 2022). The MCMC simulations were carried out with MATLAB R2020 with 1,000,000 runs and 10,000 runs for sample burn-in and a data thing of 100.

3. Results and Discussion

3.1 CO mole fractions at Mt. Kenya GAW Station and Nairobi

The results of the ~~continuous~~ CO observations at Mt. Kenya GAW station, both online and flask measurements, are presented in Figure 1. Part of the data (2002 - 2006) has been comprehensively discussed previously (Henne

et al., 2008b). ~~Part of the data (2002 – 2006) has been comprehensively discussed previously (Henne et al., 2008b), and here it will be only compared to the 2021 period with respect to a general long-term trend.~~ Overall, peak CO mole fractions were observed during the dry periods (SI Figure S1). Assessment of the long-term CO trend, following the approach by Thoning and Tans (1989), reveal a small but statistically significant positive decadal trend of 6.7 ± 0.4 ppb/10yrs. This statistical model is based on a fit function that includes a linear term, a quadratic term, as well as first and second harmonics. For comparison, simple linear regression gives a similar decadal rate of 6.2 ± 0.6 ppb/10yrs (for uncertainty estimation, see Kirago et al., 2022a). Like many types of environmental data, the present CO data display a lognormal-like concentration distribution, suggesting influence by exponential processes such as sink kinetics (Andersson, 2021). This may influence trend analysis. Similarly to linear regression, regression of log-transformed data also gives a significant positive rate, which suggests that the skewed concentration profile has little influence on trend estimation. However, given the large data gaps and different meas-urement techniques, such interpretations should not be over-emphasized. Nevertheless, the in-creasing trend here constrained for ground observations of CO is qualitatively consistent with satellite retrievals and model estimates for sub-Saharan Africa (Buchholz et al., 2021; Hedelius et al., 2021; Zheng et al., 2019). ~~However, the seasonal variations are not pronounced; the intra-seasonal peak-to-peak amplitude is larger than the variations between different seasons, implying a strong influence of short-term pollution events. Meanwhile, no clear multi-year trend in CO concentrations were detected (the rate of the long-term trend is ~ 0 ppb/year), albeit the large data gaps and different measurement techniques precludes a detailed analysis.~~

The observed CO levels, ranging between 55 – 250 ppb, are comparable to those previously recorded at Mt. Kenya station (Henne et al., 2008b), but lower than CO concentrations reported at the Rwanda Climate Observatory - another remote site also in Eastern Africa, possibly with a stronger and more direct influence of savanna burning episodes (DeWitt et al., 2019). The daytime and nighttime ambient flask CO concentrations were comparable, similar to ob-servation from Picarro-measured CO measurements though with a slight daytime elevation (SI Figure S1). During the nighttime, the station stands above the atmospheric boundary layer, hence reduced influence from local sources. Overall, changes in source strength, airmass transport pathways and meteorological parameters such as planetary boundary layer thickness are likely to be key drivers of the observed temporal variations. In Nairobi, the CO concentrations during August 2021 range between 200 – 700 ppb (~ 0.2 – 0.8 mg m-3, assuming average weather conditions), well within the WHO recommended short-term (24-h average) air quality guideline level of 4 mg m-3 (WHO, 2021). While CO is not a ma-jor direct health concern in Nairobi nor in other urban settings (Chen et al., 2021), it affects the presence of health-detrimental components such as ground-level ozone and secondary aerosols.

Back-trajectories calculated with the HYSPLIT model were combined with the CO data to learn more about source regions incident with elevated CO mole fractions. Air masses originating from different geographical areas, such as from eastern Africa, Arabian Peninsula, northern Africa, South Asia, and south-eastern Africa, as well as cleaner air masses from the Indian Ocean, are intercepted at Mt. Kenya GAW station (Figure 2). This underlines the suitability of Mt. Kenya GAW station to capture both the regional and intercontinental footprints. The elevated summertime (June - August) CO mole fractions are linked to the arrival of south-easterly airmasses, coinciding with large-scale savanna fires in southern Africa and Madagascar. The air masses shift north-easterly during winter

(December - March), and coincide with savanna fires in northern Africa (Andersson et al., 2020; Kirago et al., 2022a). Although the intercepted air masses do not directly flow over West-Central Sub-Saharan Africa, where most fires occur, the atmospheric residence time of CO is sufficient for regional and intercontinental mixing. Air masses with elevated CO loadings from South Asia and the Arabian Peninsula are also intercepted during winter. High wintertime CO amount fractions have been reported from a South Asian receptor site in the northern Indian Ocean (Dasari et al., 2022). Taken together, the seasonal variability in CO mole fraction can partly be explained by regional emission events, combined with a contribution from other geographical source regions such as South Asia.

3.2 Isotopic constraints of sources to CO from Mount Kenya and Nairobi

The stable isotope composition of CO (δ13C and δ18O) for ambient samples from Mt. Kenya GAW station during August 2021 varied temporally with the CO mole fractions (SI Figure S2). ~~The stable isotope composition of CO ($\delta^{13}C$ and $\delta^{18}O$) for ambient samples from Mt. Kenya GAW station during August 2021 varied temporally and inversely with the CO mole fractions.~~ The $\delta^{13}C$ ranged between -31.5‰ to -28.0‰, while $\delta^{18}O$ ranged between 2.5 to 10.0‰ (SI Figure S2). However, there were no distinct temporal or diurnal trends in the recorded isotopic values (both daytime and night-time samples were measured). The air masses were consistenly southeasterly during the three weeks study period (SI Figure S3). Comparable $\delta^{18}O$ composition was observed in 1996/97 samples (ranged between 3.7 to 10.4‰), but was more enriched in $\delta^{13}C$ (-28.4‰ to -26.6‰). The isotopic composition in the Mt. Kenya background region was distinct from that of the urban Nairobi location that recorded highly enriched $\delta^{18}O$ values (17.5 ± 2.2‰; SI Figure S2).

The Keeling plot approach provides insights into the regional CO sources. Here, a linear relationship is observed between the isotope signatures and the inverse of the CO amount fractions ($\delta^{13}C$ vs 1/[CO] and $\delta^{18}O$ vs 1/[CO]) both at Mt. Kenya and in Nairobi (Figure 3). This implies that the CO dynamics in this system can be described by a two-component mix-ture; a relatively stable background fraction and a regional varying source (Dasari et al., 2021; Keeling, 1958). ~~This implies that the CO dynamics in this system can be described by a two-component mixture; a relatively stable background fraction and a regional source.~~ The y-axis intercept in this relation represents the source signature. At Mt. Kenya, analysis of the recently-obtained dataset (2021) reveals the stable isotopes signature of the source of $\delta^{18}O$ = 14.0 ± 1.2‰ and $\delta^{13}C$ = -27.7 ± 0.6‰. For the samples collected during the 1996/97 campaign, the $\delta^{18}O$ signature is very similar and indistinguishable ($\delta^{18}O$ = 14.2 ± 2.1‰), while the source is more enriched in ^{13}C ($\delta^{13}C$ = -24.7 ± 0.7‰; Figure 4). The latter suggests differences in the relative strengths of the contributing sources, possibly a relatively higher contribution from C_4 plants burning or a relatively smaller influence of secondary CO from atmospheric reactions during the 1996/97 campaign It should be kept in mind that the 1990s samples were obtained at a lower altitude location on the slopes of Mt Kenya. C_4 plants like maize and sugarcane are commonly grown in Kenya, while also biomass usage (including crop residuals for household energy) and agricultural burning are prevalent in the region (World Bank, 2011). In Nairobi, a clearly distinct source signature is noted, especially for $\delta^{18}O$ ($\delta^{13}C$ = -26.0 ± 0.4‰ and $\delta^{18}O$ = 22.9 ± 0.8‰; Figures 4). The highly enriched $\delta^{18}O$ source signature in Nairobi indicates almost exclusively high temperature combustion sources, while a mixed source regime (both combustion sources and CO emanating from atmospheric reactions) is observed at Mt. Kenya; these can be quantitatively resolved using an isotopic mass balance approach

The source signatures can be used to quantitatively constrain the fractional contributions of CO in the regional background and urban atmosphere (Dasari et al., 2022). However, information was available for only two isotopes, $\delta^{13}C$ and $\delta^{18}O$, against five potential sources that can contribute to the overall CO isotopic signature (C_3 plants, fossil, C_4 plants, CH_4 oxidation and NMHC oxidation), yielding a mathematically under-determined scenario. Furthermore, the weak linear correlation for $\delta^{13}C$ in the Keeling plot ($\delta^{13}C$ vs 1/[CO]; $R^2 = 0.34$ for Mt. Kenya) limits its application in the statistical model. Therefore, only $\delta^{18}O$ signatures were here modelled ($R^2 = 0.64$ for both Mt. Kenya; $R^2 = 0.89$ for Nairobi; $P < 0.05$). Hence, the CO sources were partitioned into two major classes: primary/combustion (fossil, C_3 and C_4 biomass) and secondary (i.e., oxidation of methane and NMHC).

A Bayesian statistical model, drawing upon the model described in Dasari et al. (2022), was used to estimate the contribution of secondary ($f_{secondary}$) vs primary ($f_{primary}$) CO sources. In this model the relative contributions of primary vs. secondary CO for the temporally varying source is computed, corresponding to the $\delta^{18}O$ values at the limit where 1/CO approaches zero (the $\delta^{18}O$ intercept in the Keeling plot). First, the source end members for the two fractions were established. Unlike the oxidation of NMHC, the CH_4-oxidized CO fluxes have little variability (CH_4 has a long atmospheric lifetime) and largely contribute to the background signal (Dasari et al., 2022; Worden et al., 2019; Zheng et al., 2019). Therefore, the temporally-varying secondary CO end member was assigned that of the NMHC oxidation source ($\delta^{18}O_{secondary} = 2.4 \pm 2.4‰$).

The primary CO end member is a composite of the three combustion sources; C_4 biomass ($+20.2 \pm 4.9‰$), C_3 biomass ($+16.3 \pm 5.1‰$) and fossil fuel combustion at $+19.2 \pm 4.9‰$ (Dasari et al., 2022). Although the relative contributions are uncertain, the $\delta^{18}O$ end members largely overlap. Model estimates show biomass burning in Africa accounts for 80 - 90% of the surface CO emissions (Zheng et al., 2018). Similar contributions to black carbon (different but co-emitted incomplete combustion product) were observed using isotopic constraints with near-equal contributions from C_3 and C_4 biomass in the eastern Africa background atmosphere (Kirago et al., 2022c). Therefore, the relative source contributions were estimated at 50% from C_3 biomass and 50% from C_4 and fossil sources at Mt. Kenya. Hence, a primary CO end member was established at $\delta^{18}O_{primary} = 18.4 \pm 3.5‰$. In Nairobi, fossil fuel combustion was estimated to contribute to 85% of the CO emission in the city ($\delta^{18}O_{primary} = +19.2 \pm 4.9‰$). Since primary source endmembers largely overlap, the model simulations were generally insensitive to chosen priors, as investigated by sensitivity analysis. ~~Since individual source end members in the primary fraction largely overlap, the model simulations were generally insensitive to chosen priors, as investigated by sensitivity analysis.~~

A similar $\delta^{18}O$ source signature ($\sim 14.0 \pm 2.1‰$) was observed at the two Mt. Kenya campaigns (1996/97 and 2021). Applying the established endmembers, we estimate the contribution of CO from primary/ combustion sources at the regional background site to be at least 70%. In contrast, we found an almost exclusively primary CO component for the urban Nairobi case. Nairobi is a strong air pollution source region, and the CO loadings largely reflect the city's CO emissions. CO is, e.g., a precursor to low-level ozone, and thus emissions deteriorate air quality. Present findings show that air quality policy should target primary emissions, especially from traffic (Kirago et al., 2022b). In contrast, Mt. Kenya GAW station captures a more regional footprint with a dominant contribution from savanna fires.

4. Conclusion

This study provides ground-observational constraints that broadly supports earlier suggestions that savanna fires are the main emitters and modulators of CO loadings over Sub-Saharan Africa. Although the data gaps in CO mixing ratios and mixed instrumentation complicates detailed analysis, a small decadal increase of 6.7 ± 0.4 ppb/10yrs was resolved for the Mt. Kenya GAW station, in agreement with satellite observations and emission inventories for the Sub-Saharan region (Buchholz et al., 2021; Hedelius et al., 2021; Zheng et al., 2019). ~~Albeit data gaps in CO mixing ratios prevent detailed analysis, no clear long-term trend was resolved for the Mt. Kenya GAW station.~~ Isotope-based source apportionment shows that at least two thirds of the CO emitted from East African savanna fires are of primary origins, while for Nairobi primary sources approach 100%. The latter has implications for air quality policy, suggesting primary emissions such as traffic should be targeted, in line with previous findings for BC (Kirago et al., 2022b). These findings put constraints on satellite-based emission inventories and chemical-transport and climate modelling. Overall, this study corroborates earlier findings that in order to reduce the secondary climate warming effect from CO over Sub-Saharan Africa, man-made savanna fires should be reduced (Andersson et al., 2020).

Acknowledgement

This work was supported by research grants from the Swedish Research Council (VR contracts nos. 2013-114, 2017-05687 and 2020-05384), the Swedish Research Council for Sustainable Development (FORMAS contract no. 2020-01951), and the Swedish Research Council Distinguished Professor Grant (VR contract no. 2017-01601). Sample analysis was supported by the research grants from European Commission under the Horizon 2020 – Research and Innovation Framework Programme, H2020-INFRAIA-2020-1 (grant agreement number 101008004).

We commend the efforts of the Kenya Meteorological Department (KMD), the Swiss Federal Institute for Materials Science and Technology (Empa), and the Federal Office of Meteorology and Climatology MeteoSwiss for Mt. Kenya GAW Station operations. We appreciate the field and technical support from the staff at the Institute of Nuclear Science & Technology, University of Nairobi and KMD. We commend Prof. Carl Brenninkmeijer and Sergey Gromov for their contribution to science, and contribution to 1996/97 campaign/ data used in this manuscript.

We acknowledge the use of data from the World Data Centre for Greenhouse Gases (WDCGG) database (https://gaw.kishou.go.jp/), hosted by the World Meteorological Organization. The authors gratefully acknowledge the NOAA Air Resources Laboratory (ARL) for the provision of the HYSPLIT transport and dispersion model and/or READY website (https://www.ready.noaa.gov) used in this publication.

Author Contribution

Conceptualization of the study by AA. Design and execution of field campaigns by LK, AA, SG and MJG. Management of Mt. Kenya GAW station and instrument calibration by DN, JK, CZ, CF & MS. Isotope analysis by MEP. 1996/97 sampling campaign and sample analysis by TR. Data analysis by LK with support from AA, ÖG, SLH and SG; Manuscript writing by LK with support from co-authors.

Competing interests

The authors declare no competing interests.

Additional information

Supplementary Information (SI) contain the flask-based CO measurement data for the 1996/97 and 2021 sampling campaigns and the respective stable isotopes of CO (Table S1- S3).

Data from this study will be available in the Bolin Centre Database (bolin.su.se/data/).

References

Andersson, A.: Mechanisms for log normal concentration distributions in the environment, Sci. Rep., 11(1), 1–7, doi:10.1038/s41598-021-96010-6, 2021.

Andersson, A., Kirillova, E. N., Decesari, S., Dewitt, L., Gasore, J., Potter, K. E., Prinn, R. G., Rupakheti, M., De Dieu Ndikubwimana, J., Nkusi, J. and Safari, B.: Seasonal source variability of carbonaceous aerosols at the Rwanda Climate Observatory, Atmos. Chem. Phys., 20(8), 4561–4573, doi:10.5194/acp-20-4561-2020, 2020.

Brenninkmeijer, C. A. M.: Measurement of the abundance of 14CO in the atmosphere and the 13C/12C and 18O/16O ratio of atmospheric CO with applications in New Zealand and Antarctica, J. Geophys. Res., 98(D6), doi:10.1029/93jd00587, 1993.

Brenninkmeijer, C. A. M. and Röckmann, T.: Principal factors determining the 18O/16O ratio of atmospheric CO as derived from observations in the southern hemispheric troposphere and lowermost stratosphere, J. Geophys. Res. Atmos., 102(21), 25477–25485, doi:10.1029/97jd02291, 1997.

Brenninkmeijer, C. A. M., Röckmann, T., Bräunlich, M., Jöckei, P. and Bergamaschi, P.: Review of progress in isotope studies of atmospheric carbon monoxide, Chemosph. - Glob. Chang. Sci., 1(1–3), 33–52, doi:10.1016/S1465-9972(99)00018-5, 1999.

Buchholz, R. R., Worden, H. M., Park, M., Francis, G., Deeter, M. N., Edwards, D. P., Emmons, L. K., Gaubert, B., Gille, J., Martínez-Alonso, S., Tang, W., Kumar, R., Drummond, J. R., Clerbaux, C., George, M., Coheur, P. F., Hurtmans, D., Bowman, K. W., Luo, M., Payne, V. H., Worden, J. R., Chin, M., Levy, R. C., Warner, J., Wei, Z. and Kulawik, S. S.: Air pollution trends measured from Terra: CO and AOD over industrial, fire-prone, and background regions, Remote Sens. Environ., 256, 112275, doi:10.1016/j.rse.2020.112275, 2021.

Chen, K., Breitner, S., Wolf, K., Stafoggia, M., Sera, F., Vicedo-Cabrera, A. M., Guo, Y., Tong, S., Lavigne, E., Matus, P., Valdés, N., Kan, H., Jaakkola, J. J. K., Ryti, N. R. I., Huber, V., Scortichini, M., Hashizume, M., Honda, Y., Nunes, B., Madureira, J., Holobâcă, I. H., Fratianni, S., Kim, H., Lee, W., Tobias, A., Íñiguez, C., Forsberg, B., Åström, C., Ragettli, M. S., Guo, Y. L. L., Chen, B. Y., Li, S., Milojevic, A., Zanobetti, A., Schwartz, J., Bell,

M. L., Gasparrini, A. and Schneider, A.: Ambient carbon monoxide and daily mortality: a global time-series study in 337 cities, Lancet Planet. Heal., 5(4), e191–e199, doi:10.1016/S2542-5196(21)00026-7, 2021.

Crippa, M., Guizzardi, D., Muntean, M., Schaaf, E., Dentener, F., Van Aardenne, J. A., Monni, S., Doering, U., Olivier, J. G. J., Pagliari, V. and Janssens-Maenhout, G.: Gridded emissions of air pollutants for the period 1970-2012 within EDGAR v4.3.2, Earth Syst. Sci. Data, 10(4), 1987–2013, doi:10.5194/essd-10-1987-2018, 2018.

Dasari, S., Andersson, A., Popa, M. E., Röckmann, T., Holmstrand, H., Budhavant, K. and Gustafsson, Ö.: Observational Evidence of Large Contribution from Primary Sources for Carbon Monoxide in the South Asian Outflow, Environ. Sci. Technol., 56(1), 165–174, doi:10.1021/acs.est.1c05486, 2022.

DeWitt, H. L., Gasore, J., Rupakheti, M., Potter, K. E., Prinn, R. G., De Dieu Ndikubwimana, J., Nkusi, J. and Safari, B.: Seasonal and diurnal variability in O3, black carbon, and CO measured at the Rwanda Climate Observatory, Atmos. Chem. Phys., 19(3), 2063–2078, doi:10.5194/acp-19-2063-2019, 2019.

Duncan, B. N., Logan, J. A., Bey, I., Megretskaia, I. A., Yantosca, R. M., Novelli, P. C., Jones, N. B. and Rinsland, C. P.: Global budget of CO, 1988 - 1997: Source estimates and validation with a global model, J. Geophys. Res. Atmos., 112(22), 1988–1997, doi:10.1029/2007JD008459, 2007.

Hedelius, J. K., Toon, G. C., Buchholz, R. R., Iraci, L. T., Podolske, J. R., Roehl, C. M., Wennberg, P. O., Worden, H. M. and Wunch, D.: Regional and Urban Column CO Trends and Anomalies as Observed by MOPITT Over 16 Years, J. Geophys. Res. Atmos., 126(5), 1–18, doi:10.1029/2020JD033967, 2021.

Henne, S., Junkermann, W., Kariuki, J. M., Aseyo, J. and Klausen, J.: Mount Kenya global atmosphere watch station (MKN): Installation and meteorological characterization, J. Appl. Meteorol. Climatol., 47(11), 2946–2962, doi:10.1175/2008JAMC1834.1, 2008a.

Henne, S., Klausen, J., Junkermann, W., Kariuki, J. M., Aseyo, J. O. and Buchmann, B.: Representativeness and climatology of carbon monoxide and ozone at the global GAW station Mt. Kenya in equatorial Africa, Atmos. Chem. Phys., 8(12), 3119–3139, doi:10.5194/acp-8-3119-2008, 2008b.

Keeling, C. D.: The concentration and isotopic abundances of atmospheric carbon dioxide in rural areas, Geochim. Cosmochim. Acta, 13(4), 322–334, doi:10.1016/0016-7037(58)90033-4, 1958.

Kirago, L., Gustafsson, Ö., Gaita, S. M., Haslett, S. L., deWitt, H. L., Gasore, J., Potter, K. E., Prinn, R. G., Rupakheti, M., Ndikubwimana, J. de D., Safari, B. and Andersson, A.: Atmospheric Black Carbon Loadings and Sources over Eastern Sub-Saharan Africa Are Governed by the Regional Savanna Fires, Environ. Sci. Technol., doi:10.1021/acs.est.2c05837, 2022a.

Kirago, L., Gatari, M. J., Gustafsson, Ö. and Andersson, A.: Black carbon emissions from traffic contribute substantially to air pollution in Nairobi, Kenya, Commun. Earth Environ., 3(1), 1–8, doi:10.1038/s43247-022-00400-1, 2022b.

~~Kirago, L., Gatari, M. J., Gustafsson, Ö. and Andersson, A.: Large Contribution of Fossil Black Carbon to Air~~

~~Pollution in Nairobi , Kenya, Commun. Earth Environ., 2022c.~~

Kulmala, M.: Build a global Earth observatory, Nature, 553(7686), 21–23, doi:10.1038/d41586-017-08967-y, 2018.

Lelieveld, J., Gromov, S., Pozzer, A. and Taraborrelli, D.: Global tropospheric hydroxyl distribution, budget and reactivity, Atmos. Chem. Phys., 16(19), 12477–12493, doi:10.5194/acp-16-12477-2016, 2016.

Mak, J. E. and Brenninkmeijer, C. A. M.: Compressed air sample technology for isotopic analysis of atmospheric carbon monoxide, J. Atmos. Ocean. Technol., 11(2), 425–431, doi:https://doi.org/10.1175/1520-0426(1994)011%3C0425:CASTFI%3E2.0.CO;2, 1994.

Pathirana, S. L., Van Der Veen, C., Popa, M. E. and Röckmann, T.: An analytical system for stable isotope analysis on carbon monoxide using continuous-flow isotope-ratio mass spectrometry, Atmos. Meas. Tech., 8(12), 5315–5324, doi:10.5194/amt-8-5315-2015, 2015.

Popa, M. E., Vollmer, M. K., Jordan, A., Brand, W. A., Pathirana, S. L., Rothe, M. and Röckmann, T.: Vehicle emissions of greenhouse gases and related tracers from a tunnel study: CO : CO2, N2O : CH4 : O2 : Atios, and the stable isotopes 13C and 18O in CO2 and CO, Atmos. Chem. Phys., 14(4), 2105–2123, doi:10.5194/acp-14-2105-2014, 2014.

Röckmann, T., Brenninkmeijer, C. A. M., Saueressig, G., Bergamaschi, P., Crowley, J. N., Fischer, H. and Crutzen, P. J.: Mass-independent oxygen isotope fractionation in atmospheric CO as a result of the reaction CO + OH, Science (80-.)., 281(5376), 544–546, doi:10.1126/science.281.5376.544, 1998.

Röckmann, T., Jöckel, P., Gros, V., Bräunlich, M., Possnert, G. and Brenninkmeijer, C. A. M.: Using 14C, 13C, 18O and 17O isotopic variations to provide insights into the high northern latitude surface CO inventory, Atmos. Chem. Phys., 2, 147–159 [online] Available from: www.atmos-chem-phys.org/acp/2/147/, 2002.

Stein, A. F., Draxler, R. R., Rolph, G. D., Stunder, B. J. B., Cohen, M. D. and Ngan, F.: Noaa's hysplit atmospheric transport and dispersion modeling system, Bull. Am. Meteorol. Soc., 96(12), 2059–2077, doi:10.1175/BAMS-D-14-00110.1, 2015.

Szopa, S., Naik, V., Adhikary, B., Artaxo, P., Berntsen, T., Collins, W. D., Fuzzi, S., Gallardo, L., Kiendler, A., Scharr, Z., Klimont, Liao, H., Unger, N. and Zanis, P.: Short-Lived Climate Forcers. In Climate Change 2021: The Physical Science Basis. Contribution of Working Group I to the Sixth Assessment Report of the Intergovernmental Panel on Climate Change. [online] Available from: https://www.ipcc.ch/, 2021.

Thoning, K. W. and Tans, P. P.: Atmospheric carbon dioxide at Mauna Loa Observatory. 2. Analysis of the NOAA GMCC data, 1974-1985, J. Geophys. Res., 94(D6), 8549–8565, doi:10.1029/JD094iD06p08549, 1989.

WHO: WHO Expert Consultation: Available evidence for the future update of the WHO Global Air Quality Guidelines, Copenhagen, Denmark. [online] Available from: http://www.euro.who.int/pubrequest, 2016.

WHO: WHO Global Air Quality Guidelines. Particulate matter (PM2.5 and PM10), ozone, nitrogen dioxide, sulfur dioxide and carbon monoxide., 2021.

Worden, H. M., Anthony Bloom, A., Worden, J. R., Jiang, Z., Marais, E. A., Stavrakou, T., Gaubert, B. and Lacey, F.: New constraints on biogenic emissions using satellite-based estimates of carbon monoxide fluxes, Atmos. Chem. Phys., 19(21), 13569–13579, doi:10.5194/acp-19-13569-2019, 2019.

World Bank: Wood-Based Biomass Energy Development for Sub-Saharan Africa, Washington, D.C., 2011.

Zellweger, C., Hüglin, C., Klausen, J., Steinbacher, M., Vollmer, M. and Buchmann, B.: Inter-comparison of four different carbon monoxide measurement techniques and evaluation of the long-term carbon monoxide time series of Jungfraujoch, Atmos. Chem. Phys., 9(11), 3491–3503, doi:10.5194/acp-9-3491-2009, 2009.

Zellweger, C., Steinbacher, M. and Buchmann, B.: GAW Report No. 256 / WCC-Empa Report No. 19/4. System and Performance Audit of Surface Ozone, Carbon Monoxide, Methane, and Carbon Dioxide at the Global GAW Station Mt. Kenya, Kenya, Geneva. [online] Available from: https://library.wmo.int/index.php?lvl=notice_display&id=21780, 2020.

Zhang, J. J., Wei, Y. and Fang, Z.: Ozone pollution: A major health hazard worldwide, Front. Immunol., 10(OCT), 1–10, doi:10.3389/fimmu.2019.02518, 2019.

Zheng, B., Chevallier, F., Ciais, P., Yin, Y. and Wang, Y.: On the Role of the Flaming to Smoldering Transition in the Seasonal Cycle of African Fire Emissions, Geophys. Res. Lett., 45(21), 11,998-12,007, doi:10.1029/2018GL079092, 2018.

Zheng, B., Chevallier, F., Yin, Y., Ciais, P., Fortems-Cheiney, A., Deeter, M. N., Parker, R. J., Wang, Y., Worden, H. M. and Zhao, Y.: Global atmospheric carbon monoxide budget 2000-2017 inferred from multi-species atmospheric inversions, Earth Syst. Sci. Data, 11(3), 1411–1436, doi:10.5194/essd-11-1411-2019, 2019.

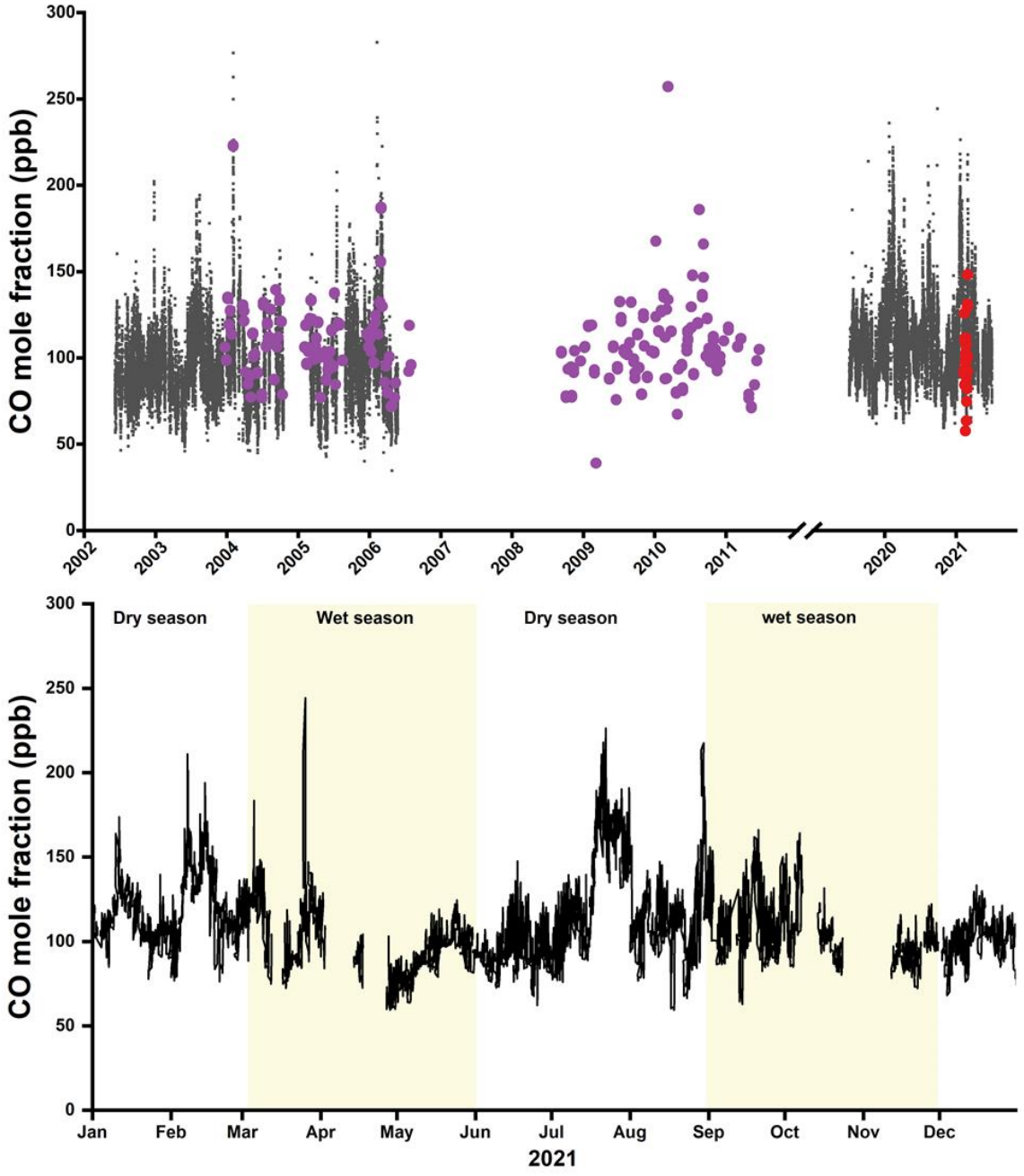

441

442 ~~Figure 1: Time series of CO mole fractions at Mt. Kenya GAW station. a) Daily resolution~~

443 ~~continuously measured CO mole fraction (Picarro) at Mt. Kenya GAW is represented by black dots.~~

444 ~~The CO data was retrieved from the WMO's-WDCGG database covering 2002 to 2021. Different~~

445 ~~instrumentations were used over time, but similar instrumental calibration, quality control, and~~

446 ~~assurance protocols were applied. Flask-based measurements by NOAA at the station are presented~~

447 ~~in purple symbols, while flask samples during our 2021 campaign are shown in red symbols. b)~~

448 ~~Variations in CO mole fractions for the year 2021. The prevailing typical weather conditions are~~

~~indicated.~~

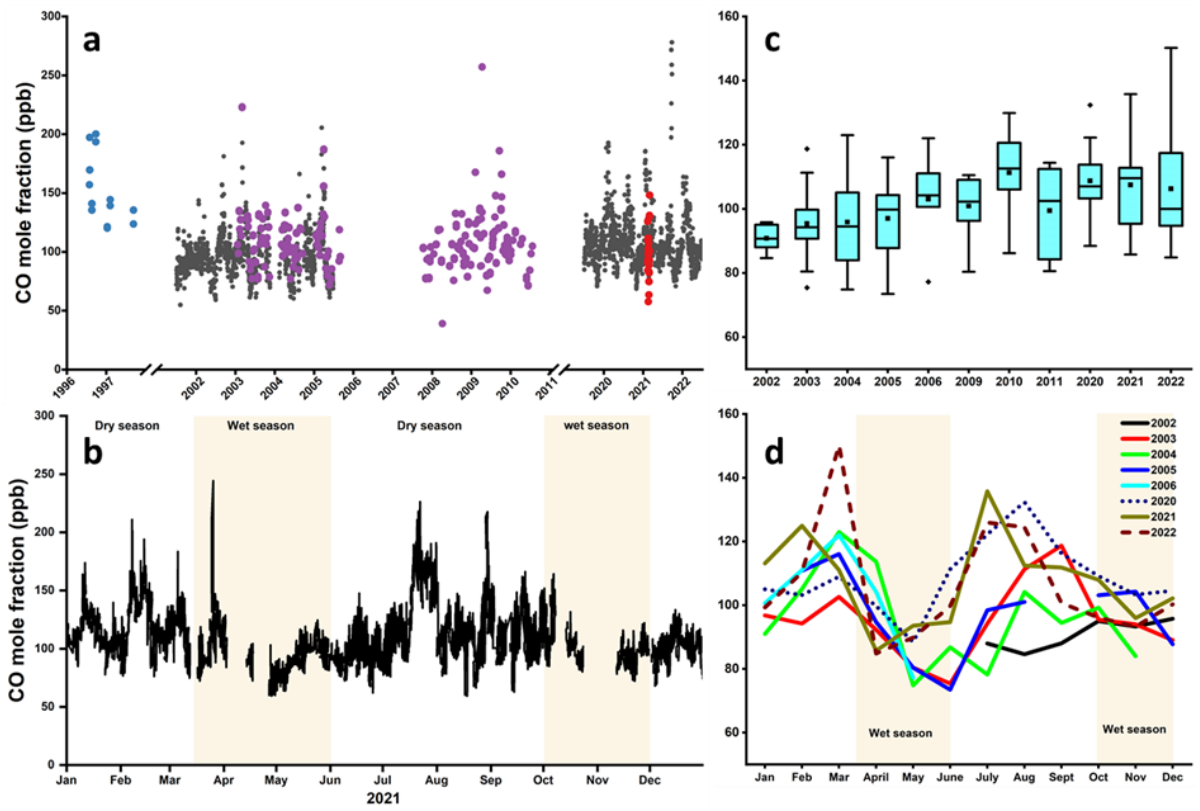

Figure 1: Time series of CO mole fractions at Mt. Kenya GAW station. a) Daily-resolution continuously measured CO mole fraction (Picarro) at Mt. Kenya GAW is represented by black dots. The CO data was retrieved from the WMO's-WDCGG database covering 2002- 2021. Different instrumentations were used over time, but similar instrumental calibration, quality control, and assurance protocols were applied. Flask-based measurements by NOAA at the station are presented in purple symbols, while flask samples during 1996/97 campaigns are shown as blue dots and flask samples from the 2021 campaign are shown in red symbols, in good agreement with the online measurements, as shown in SI Figure S4. b) Variations of CO mole fractions for the year 2021. The prevailing typical weather conditions are indicated. c) Annual averaged CO mixing ratios. The boxes represent the 25th and 75th quantiles, and the black line represents the median value. The bottom/top whiskers are the minimum and maximum values, respectively, while diamonds represent the outliers. d) Inter-annual cycles of monthly averaged CO mole fractions (coloured lines represent individual years).

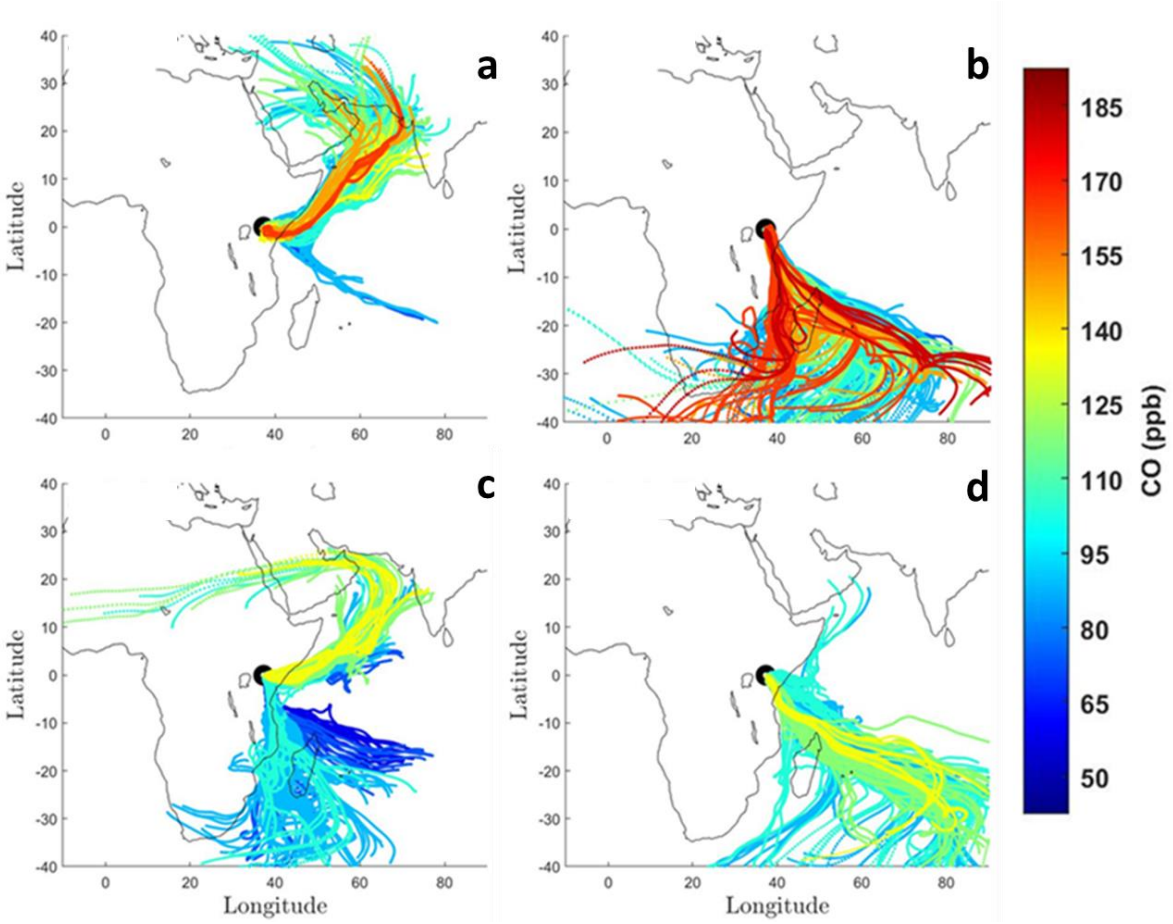

Figure 2: Seasonal changes in CO concentration-coded back trajectories intercepted at Mt. Kenya; (a) December – February 2021, (b) June – August 2021, (c) March – May 2021, and (d) Sep-tember – November 2021. (a) December – February, (b) June – August, (c) March – May, and (d) September – November. Ten days air masses back trajectories are calculated at an arrival height of 100 m above ground level.

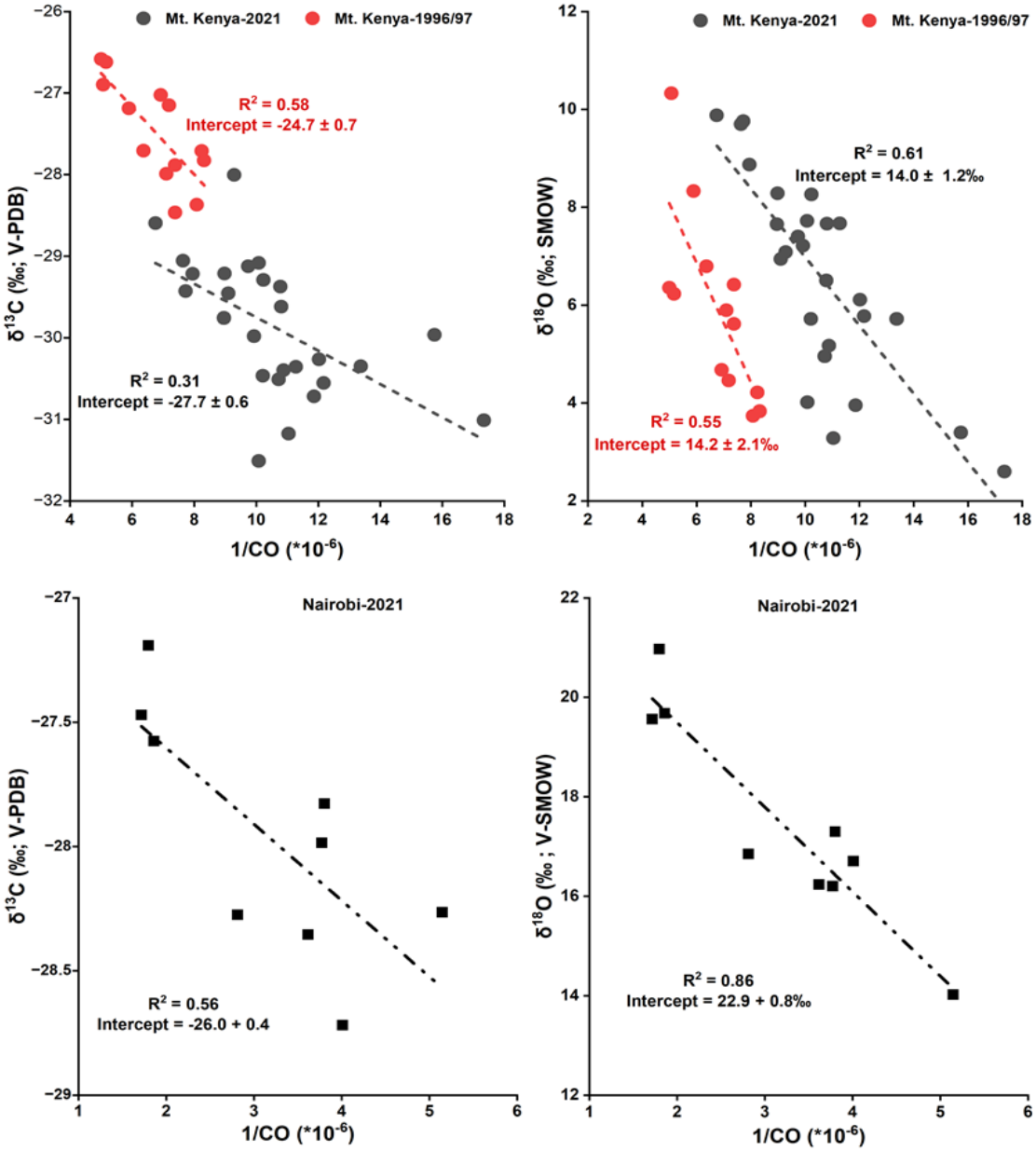

~~Figure 3: The Keeling relation plots (i.e., isotopic signature vs the inverse of the measured CO mole fraction) for Mt. Kenya (top panel) and Nairobi (bottom panel). The y intercept in the Keeling relationship represents the source signature.~~

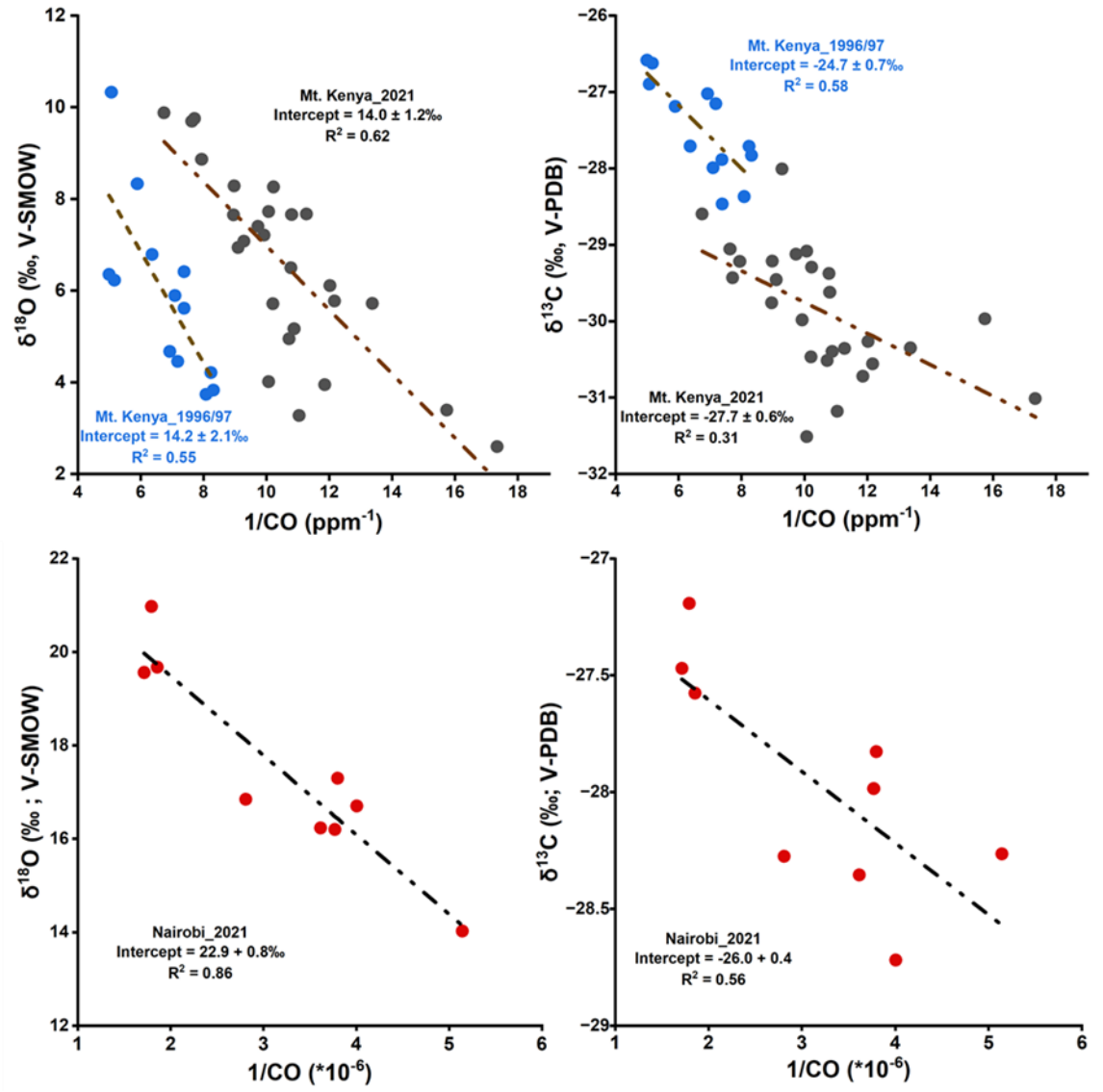

Figure 3: The Keeling relation plots (i.e., signatures of the two isotopic systems vs the inverse of the measured CO mole fraction) for Mt. Kenya (top panel) and Nairobi (bottom panel). The y-intercept in the Keeling relationship represents the source signature.

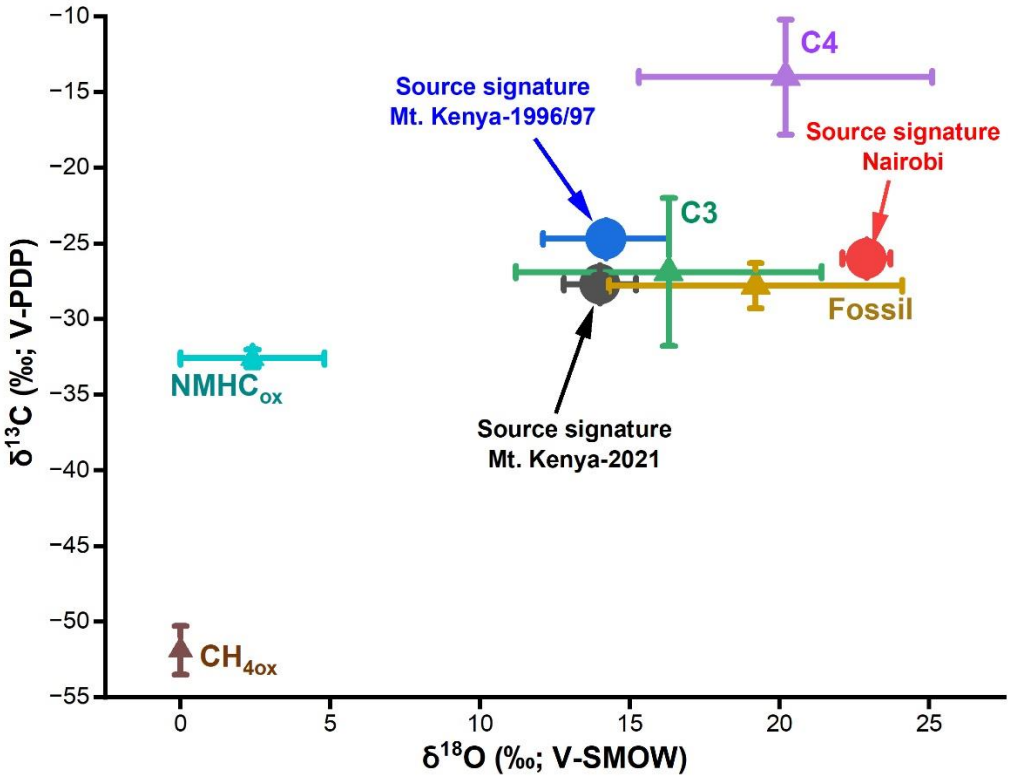

476

477 **Figure 4: Stable isotope (δ^{13}C and δ^{18}O) source signatures of CO for Nairobi and Mt. Kenya (2021 and 1996/97), and**
478 **the source end members. The source end members are adopted from Brenninkmeijer et al. (1999).**